

Class Incremental Learning with Task-Specific Batch Normalization and Out-of-Distribution Detection

Xuchen Xie^{1,3}, Yiqiao Qiu^{4†‡}, Run Lin^{1,3†}, Weishi Zheng^{1,3}, and Ruixuan Wang^{1,2,3*}

¹School of Computer Science and Engineering, Sun Yat-sen University, Guangzhou, China

²Peng Cheng Laboratory, Shenzhen, China

³Key Laboratory of Machine Intelligence and Advanced Computing, MOE, Guangzhou, China

⁴Department of Computer Science and Engineering, University of California San Diego, United States

Abstract—This study focuses on incremental learning for image classification, exploring how to reduce catastrophic forgetting [1] of all learned knowledge when access to old data is restricted due to memory or privacy constraints. The challenge of incremental learning lies in achieving an optimal balance between plasticity, the ability to learn new knowledge, and stability, the ability to retain old knowledge. Based on whether the task identifier (task-ID) of an image can be obtained during the test stage, incremental learning for image classification is divided into two main paradigms, which are task incremental learning (TIL) and class incremental learning (CIL). The TIL paradigm has access to the task-ID, allowing it to use multiple task-specific classification heads selected based on the task-ID. Consequently, in CIL, where the task-ID is unavailable, TIL methods must predict the task-ID to extend their application to the CIL paradigm. Our previous method [2] for TIL adds task-specific batch normalization and classification heads incrementally. This work extends the method by predicting task-ID through an “unknown” class added to each classification head. The head with the lowest “unknown” probability is selected, enabling task-ID prediction and making the method applicable to CIL. The task-specific batch normalization (BN) modules effectively adjust the distribution of output feature maps across different tasks, enhancing the model’s plasticity. Moreover, since BN has much fewer parameters compared to convolutional kernels, most of the feature extractor’s parameters remain unchanged. By only modifying the BN layers as new tasks arrive, the model can effectively manage parameter growth while ensuring stability across tasks. In summary, the proposed method can efficiently control parameter growth while ensuring both the model’s plasticity and stability. The innovation of this study lies in the first-time introduction of task-specific BN into CIL and verifying the feasibility of extending TIL methods to CIL through task-ID prediction. Our method achieves state-of-the-art performance on two medical image datasets and one natural image dataset. The source code will be released publicly.

Index Terms—Task Incremental Learning, Class Incremental Learning, Batch Normalization, Out-of-Distribution Detection

I. INTRODUCTION

DEEP learning models have been extensively applied to various fields. However, they usually rely on large amounts of data for training to achieve high performance. In real-world scenarios, it is often difficult to obtain data for all

necessary classes at once, leading to data arriving in multiple phases. Moreover, the classes appearing in different phases are typically non-overlapping. Consequently, AI models often need to learn new classes gradually. With privacy and memory constraints, models can only access data from the current phase and are restricted to retrieve data from previous phases. Research has found that under these circumstances, models are susceptible to catastrophic forgetting [1], a phenomenon characterized by a substantial decline in performance on previously learned tasks. Therefore, enabling models to continually learn new knowledge without forgetting old knowledge is one key challenge for promoting the widespread application of deep learning based AI across various fields.

Several methods have been proposed to alleviate catastrophic forgetting. However, these current methods often struggle to balance the model’s stability [3] (ability to retain old knowledge) and plasticity [3] (ability to learn new knowledge), and they also face challenges in controlling parameter growth. For instance, methods based on model parameter regularization [3]–[5] aim to protect crucial neural network weights from being updated drastically through constraints, thus preventing old knowledge loss. However, this protection can lead to model rigidity, making it difficult for the model to assimilate new knowledge. Another type of method is the dynamic expansion of the model’s structure [6]–[10], where new layers or sub-modules are added for new tasks. Although such method significantly enhances the model’s plasticity, it inevitably increases memory demands. Therefore, effectively adding network components without substantially increasing the memory burden is a fundamental issue for this type of method. Overall, existing methods struggle to achieve a good balance between plasticity, stability and memory control, which is the core challenge in incremental learning.

During training on new tasks, because of the distinctive knowledge representations between tasks, the unrestricted continuous changes in feature extractor parameters is the key factor leading to catastrophic forgetting. Thus, minimizing updates of the feature extractor can substantially mitigate or completely avoid catastrophic forgetting. Based on the idea of minimizing changes to the learned knowledge representation inside the feature extractor, we propose a method utilizing

† Authors contributed equally.

‡ Works not related to role at Amazon.

* Corresponding author: wangruix5@mail.sysu.edu.cn

task-specific Batch Normalization [11] (BN) and classification heads. In classic deep convolutional networks like ResNet [12], the number of parameters of BN and classification heads is negligible comparing with convolution layers. Thus we can add these additional task-specific modules without concerning parameters explosion issue like DynaER [9] throughout incremental learning. This method also prevents the erasing of existing knowledge related to old tasks because only these new BN and classification head modules are trainable, thereby avoiding catastrophic forgetting and ensuring model stability. Moreover, since BN is able to reshape the data distribution, its powerful expressive capability has been demonstrated in the field of GAN [13]. Therefore, by introducing task-specific BN, the model’s ability to learn the distribution of different tasks can be greatly enhanced, improving the model’s plasticity.

This paper is an extension of our previously published conference paper [2], which utilized task-specific batch normalization in TIL. In this study, we further incorporate out-of-distribution detection, extending the method to CIL paradigm. Overall, our contributions are listed below:

- 1) We introduce task-specific batch normalization in the CIL paradigm for the first time.
- 2) Building on multiple task-specific classification heads, we introduce out-of-distribution detection for task-ID prediction, demonstrating the effectiveness of using task-ID prediction approach to extend TIL method for CIL, where task-ID is unknown.
- 3) Our proposed method achieves state-of-the-art classification performance on two medical image datasets and one natural image dataset, outperforming existing methods in overall performance and achieving a better balance among model stability and plasticity, and parameter growth.

II. RELATED WORK

A. General Overview

Incremental learning for image classification is divided into two main paradigms, i.e., task incremental learning [14], [15] (TIL) and class incremental learning [14], [15] (CIL), as the task-ID is provided in the test stage of TIL, but not for CIL. The diagrams of these two paradigms are shown in Figure 1. In the TIL paradigm, the model typically includes a shared feature extractor and multiple task-specific classification heads. During testing, the appropriate classification head is selected based on the known task-ID. In contrast, CIL typically employs a shared feature extractor across all tasks but maintains a single, unified classification head. This head progressively increases in channel dimensions as new tasks are introduced, ensuring its output can cover all classes of all tasks.

Methods from CIL can be transferred to TIL by focusing only on specific categories associated with the task-ID during testing. However, adapting methods from TIL to CIL remains a significant challenge, mainly because choosing the correct classification head from multiple options to make the final prediction becomes particularly challenging without task-ID. Thus, for most existing methods, the main difference

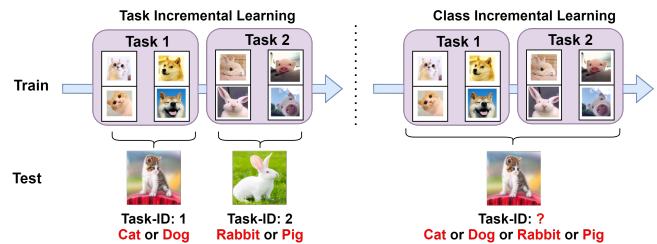


Fig. 1: The two main paradigms of incremental learning for image classification: task incremental learning (with task-ID available during testing) and class incremental learning (without task-ID during testing).

between these two paradigms lies in that TIL paradigm has multiple classification heads specific to certain tasks, while CIL paradigm typically have only one classification head that adapts to all tasks. CIL does not require task-ID as prior knowledge, making it more aligned with practical applications. Therefore, this paper focuses on CIL and introduces methods related to CIL.

Class Incremental Learning (CIL) Many methods have been proposed to directly address the catastrophic forgetting problem in the CIL domain, including [3]–[5], [9], [16]–[18]. Most existing methods can be categorized into four types.

The first type is regularization-based, such as EWC [4], MAS [5], and RWalk [3], which measure the importance of model parameters and restrict the updates of crucial parameters to prevent forgetting. However, these methods constrain model updates, limiting the model’s learning capacity and often hindering performance on new tasks.

The second type is distillation-based, where knowledge from old models is distilled into new models by forcing the features from new models similar to that from old models, such as the well-known LwF [19], PODNet [20], WA [21] and UCIR [22]. The key component in these methods is some distillation functions applied between the output of same layers from the old and new models, like some intermediate feature map or logit. The gradient of distillation loss forces new models to generate visual representations similar to that of old models, thus retaining old knowledge and avoiding forgetting. However, as tasks accumulate, knowledge retention diminishes, and the effectiveness of distillation becomes limited because the source (old model from the previous stage) being distilled cannot precisely represent the knowledge from the earliest tasks.

The third type of methods is replay-based, which alleviate model forgetting by replaying a small portion of real or synthetic old samples, including iCaRL [23], CF-IL [24], DER++ [25] and GSS [26]. Most existing methods also rely on replay, such as knowledge distillation-based methods, which typically require replaying old samples to enhance the distillation effects. However, in incremental learning paradigms where tasks are presented with infinite data streams, storage and memory are always limited. Therefore, how to effectively select and utilize the representative samples for old sample

replay is worth exploring.

The fourth type is expansion-based, continuously expanding the model to enhance expressive capabilities, such as PNN [6], PathNet [7] and DyTox [8]. A typical example of this type of method is DynaER [9]. DynaER introduces new learnable feature extractors with the arrival of new tasks to incorporate additional feature dimensions. This method of adding feature extractors effectively enhances the model’s expressive capacity, allowing it to achieve SOTA performance when it was proposed. However, with the arrival of new tasks, the expansion of the feature extractor significantly increases the number of parameters. This is not only a limitation of the DynaER method but also a challenge for this category of methods, i.e., how to add relatively few and efficient components as new tasks arrive, ensuring performance without burdening memory too much.

CIL through Task-ID Prediction The characteristic of this type of method is the use of additional task-ID prediction to extend TIL methods to CIL. In this category of methods, early attempts include CCG [27], which constructed a separate network to predict task-ID, while HyperNet [28] and PR-Ent [29] used entropy metrics to predict task-ID. The performances of these methods are not satisfactory, and some of these methods also face practical application issues. For example, iTAML [30] requires that the data in the same batch come from the same task during testing, which clearly does not meet the needs of real-world applications. Overall, these early methods, though exploratory, have limitations in both performance and practical application. These issues originate from a lack of theoretical guidance, leading to a failure to recognize that enhancing a model’s OOD detection capability is crucial for effective task-ID prediction. Kim et al. [31] examined the limitations of previous methods and provided theoretical guidance for the first time. They proposed that under conditions with multiple classification heads, the CIL problem can be effectively divided into two sub-problems: task-ID prediction (TP) and within-task prediction (WP). The overall accuracy of CIL is actually determined by the multiplication of WP and TP accuracy. In CIL, TP is essential because the task-ID is not provided during testing. WP refers to predicting the specific class within the task after the task-ID has been predicted, which is equivalent to TIL. Furthermore, they pointed out that better OOD performance can contribute to improved TP performance, as the model must establish decision boundaries between new and old tasks to effectively detect OOD samples for each task. To facilitate the TP performance, some recently advanced OOD methods like Mahalanobis [32], Energy [33], and HIMPLoS [34] can be applied to help making TP decision in the TIL model. For example, MORE [35] uses a pretrained ImageNet1000 [36] model as the base and incorporates task-specific masked adapters into the Transformer blocks, which are trained when new tasks arrive while freezing the main parameters of the model. During testing, it utilizes the Softmax output values and corrects them using the Mahalanobis distance between features and class centroids to perform task-ID prediction. The total number of model parameters is fixed, and training task-specific masks reduces the learnable parameters

available for subsequent tasks, thereby affecting the learning ability on these tasks, especially when the number of tasks is numerous. Additionally, when the number of samples per class is small, the estimated centroid of each class may not be accurate, thereby affecting the effectiveness of score correction.

In conclusion, this area of research is relatively new as its exploratory theoretical support and performance guarantees are gradually emerging. These methods hold a broad research prospect, particularly by enhancing the accuracy of TP during testing, which is expected to further improve performance. However, the similarity between tasks may pose challenges for task-ID prediction, necessitating further in-depth research and resolution.

III. METHOD

The schematic diagram of the method is shown in Figure 2. Figure 2(a) and Figure 2(b) represent the training stage, which are executed sequentially as Figure 2(a)→ Figure 2(b). Figure 2(a) depicts the first stage of training, where task-specific batch normalization and classification heads are added as new tasks arrive, and the “unknown” class is added to the classification heads. Each task corresponds to a task-specific sub-model, where each sub-model consists of task-shared convolutional kernels, task-specific BN, and task-specific classification head. Figure 2(b) represents the second stage of training, where the out-of-distribution detection capabilities of the sub-models are aligned. Figure 2(c) illustrates the test stage, under the existence of multiple task-specific sub-models, task-ID prediction is performed first, followed by within-task prediction to obtain the final prediction.

A. Task-Specific Batch Normalization and Heads

The powerful expressive capability of batch normalization was discovered early in research work about generative adversarial networks (GAN) [13], [37], where Karras et al. discovered that the StyleGAN model is able to generate a variety of realistic images by just merely adjusting the BN layer. Specifically, for the l^{th} layer’s j^{th} convolutional kernel within the convolutional neural network, we denote the output of the convolution operation on a single input sample as feature map $\mathbf{z}_{l,j}$. Across a batch, the outputs of all input samples for this kernel are marked as $\mathbf{Z}_{l,j}$. The BN layer standardizes each feature map as follows

$$q_{l,j}(\mathbf{z}_{l,j}) = \gamma_{l,j} \frac{\mathbf{z}_{l,j} - \mu(\mathbf{Z}_{l,j})}{\sigma(\mathbf{Z}_{l,j})} + \beta_{l,j}, \quad (1)$$

where $\mu(\mathbf{Z}_{l,j})$ and $\sigma(\mathbf{Z}_{l,j})$ denote the mean and standard deviation of all elements within the feature map produced by the j^{th} convolutional kernel of the l^{th} layer. $\gamma_{l,j}$ and $\beta_{l,j}$ are trainable scaling and shifting parameters that independently adjust each feature map. This means that BN first normalizes the outputs to zero mean and unit variance and then re-adjusts the distribution of the feature maps through scaling and shifting operations. This mechanism shows that the parameters of the BN layer are directly related to the data distribution, enhancing the feature extractor’s adaptability

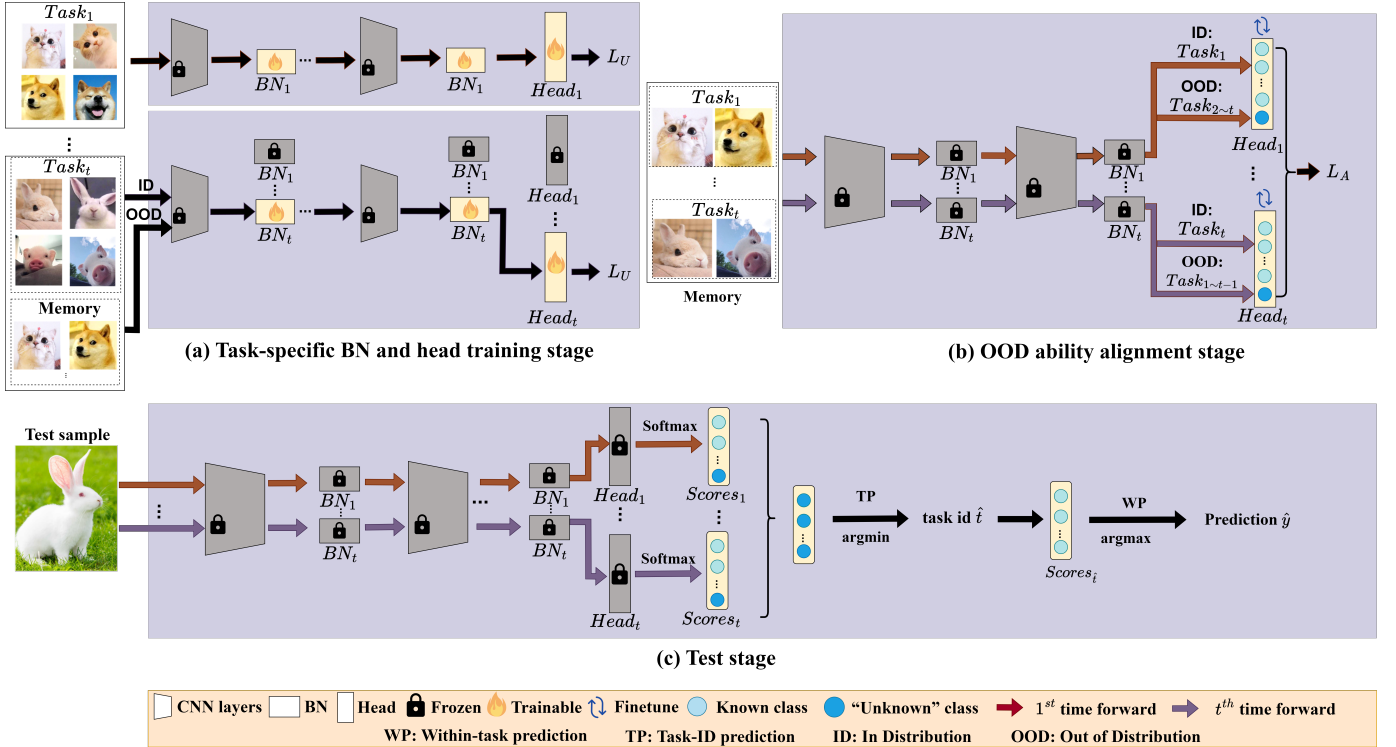


Fig. 2: Framework of our proposed method. Sub-figures (a) and (b) depict the training stage. Sub-figure (a) shows the process of gradually adding and training task-specific BN layers and classification heads as new tasks arrive. After each task is completed, the OOD capability alignment stage, as shown in sub-figure (b), is conducted. Sub-figure (c) presents the test stage, which starts by identifying the classification head with the lowest output probability of the “unknown” class for task-ID prediction (TP) and finally performing within-task prediction (WP) on these outputs.

for different task data distributions. Moreover, compared to the numerous parameters in convolutional kernels, the BN layer has much fewer parameters, which not only makes it easier to adjust but also more storage-efficient. For example, in the ResNet18 model, the total parameter number of all convolutional kernels is 11 million parameters, but all the BN layers contain only about 15,000 parameters, much fewer than that of all convolutional kernels.

Given the benefits of BN layers in improving expressiveness and facilitating parameter control, we propose the following method, which constitutes a part of our method: after obtaining a strong feature extractor through pretraining, we progressively add and train task-specific BN layers and classification heads for sequentially arrived new tasks. Due to the small number of parameters, these learned task-specific BN parameters and classification heads can be stored throughout all incremental learning stages. This strategy is not only efficient in terms of storage but also enhances the learning capability of the feature extractor for each task through the robust expressive power of the BN layers.

The following provides a symbolic representation of how the proposed method augments the relevant elements of the model as tasks arrive in the framework of incremental learning. In the framework of incremental learning, data arrive in T tasks, with each task associated with a specific dataset, represented as $\mathbf{D}_1, \mathbf{D}_2, \dots, \mathbf{D}_T$. In the feature extractor, the convolutional kernels, primarily responsible for extracting im-

age features, are parameterized by ϕ . The batch normalization, responsible for standardizing the output of convolutions, is parameterized by ω_t . With the arrival of new task t , the convolutional kernel parameters ϕ remain fixed and do not participate in training. The introduction of a new task results in the addition and training of BN layer parameters ω_t and the corresponding classification head h_t . Therefore, after completing the training for task t , the feature extractor will include one ϕ and t ω_t s. By combining ϕ with each ω_t and h_t , the model effectively forms T distinct sub-models, with each sub-model specialized for a specific task. The t -th sub-model, denoted as S_t , is thus responsible for handling task t , utilizing the corresponding batch normalization parameters and classification head.

B. “Unknown” Class in Classification Heads

Our method employs multiple task-specific classification heads for class incremental learning. Due to the unknown task-ID in test stage, it is necessary to first perform task-ID Prediction (TP) to select a task head, and then proceed with within-task Prediction (WP) to achieve the final prediction. The test stage is illustrated in Figure 2(c). The accuracy of TP directly affects whether the task that contains ground-truth class of the test sample is selected, and an incorrect selection renders WP ineffective. Moreover, the accuracy of WP indicates the ability to accurately classify within the task once the appropriate task head has been correctly chosen. Thus, the

effectiveness of the proposed method fundamentally depends on the multiplication of WP accuracy and TP accuracy. The reason for using task-specific BN and heads is to ensure the performance of WP through its powerful expressiveness. Additionally, the performance of TP also needs improvement. To make TP perform well, each task-specific sub-model S_t for \mathbf{D}_t must have the capability to detect out-of-distribution samples. This capability enables the model to effectively differentiate between samples from the in-distribution dataset \mathbf{D}_t and those from datasets considered out-of-distribution for the current task t (i.e., \mathbf{D}_k where $k \neq t$), thereby establishing clear decision boundaries both within and across tasks.

To equip each sub-model with OOD detection capability, we incorporate the concept of the “unknown” class from the classical OpenMax [38] method into our model architecture. Similar to OpenMax, we extend the classification output vector by adding an “unknown” class to the classification head. If the output for the “unknown” class is the highest among all outputs for a given sample, the sample is classified as an OOD sample. For the new task-specific sub-model, an OOD-replay step is performed using a small number of old task samples which are stored in memory. Let \mathbf{M}_{t-1} denote the memory set containing a limited number of samples from the $t-1$ previous tasks, and \mathbf{D}_t the new task sample set consisting of C_t classes. In the classification head h_t for task t , the (C_t+1) -th class is introduced as the “unknown” class. The parameters trained during task t are $\theta_t = \{\omega_t, h_t\}$, and the corresponding loss function is defined as

$$L_U(\theta_t) = -\frac{1}{|\mathbf{D}_t|} \sum_{(\mathbf{x}_i, y_i) \in \mathbf{D}_t} \log p(y_i | \mathbf{x}_i; \phi, \omega_t, h_t) - \frac{1}{|\mathbf{M}_{t-1}|} \sum_{\mathbf{x}_j \in \mathbf{M}_{t-1}} \log p(C_t + 1 | \mathbf{x}_j; \phi, \omega_t, h_t), \quad (2)$$

where \mathbf{x}_i and y_i represent i -th sample and its label from task t , while \mathbf{x}_j represents the j -th old sample from the memory \mathbf{M}_{t-1} . By adding an “unknown” class to the classification head, the output probability of the “unknown” class in the head can be used as metric to perform TP. During the test stage, after the input is passed through the sub-models of all tasks, the task head with the smallest output for the “unknown” class is first selected (TP). Then, within-task prediction (WP) is performed on the selected task’s classification output vector to obtain the final class prediction.

C. OOD Detection Capability Alignment Stage

During the training of BN and classification heads, samples from old tasks are mapped towards the “unknown” class in the new classification head. Although the memory can only store a limited number of old task samples for replay, the number of old task classes in the memory gradually increases as new tasks arrive. This means that sub-models specific to later tasks encounter a broader range of old task sample classes. For instance, in the sub-model corresponding to the first task, there are no old task samples in the memory, while the sub-model for the final task has access to samples from all previous task classes. This imbalance can lead to variations in

the “unknown” scores output by different task-specific sub-models, resulting in inconsistent confidence outputs and a decrease in task identification prediction accuracy. To address this challenge, an OOD detection capability alignment stage is introduced to fine-tune each task-specific classification head.

Specifically, this stage is added after training the BN layers and the classification head for the new task, as shown in Figure 2(b). During this stage, the feature extractor remains fixed, only the parameters of the classification heads are updated. Taking the t -th task as an example, herding selection [23] is first used to select a small number of samples from the t -th task, updating \mathbf{M}_{t-1} to \mathbf{M}_t is to ensure that it covers the past t tasks. Subsequently, \mathbf{M}_t is used to train all classification heads from 1 to t . The corresponding loss function is defined as follows

$$L_A(\theta_t) = \frac{1}{|\mathbf{M}_t|t} \sum_{j=1}^t \sum_{(\mathbf{x}_i, y_i) \in \mathbf{M}_t} \left[-1[\mathbf{x}_i \in \mathbf{D}_j] \log p(y_i | \mathbf{x}_i; \phi, \omega_j, h_j) - 1[\mathbf{x}_i \notin \mathbf{D}_j] \log p(C_j + 1 | \mathbf{x}_i; \phi, \omega_j, h_j) \right], \quad (3)$$

for each stored head h_j , the samples in memory \mathbf{M}_t related to task j correspond to the known classes 1 through C_j and are optimized using their respective labels. Samples from other tasks are associated with the “unknown” class, denoted as class $C_j + 1$, in the classification head h_j . This ensures that each task-specific sub-model is exposed to an equal number of OOD classes, enhancing the OOD detection capability of each sub-model and ensuring the same level of OOD detection capability is retained across all sub-models.

D. Comparison to Related Methods

Using task-ID prediction to extend TIL methods to CIL has been explored in several existing methods, but our study differs in several key aspects. The earliest theoretical work to propose enhancing model OOD performance to improve TP performance was conducted by Kim et al. [31]. This work combines the TIL method HAT [39] with the contrastive learning method CSI [40], achieving favorable results. MORE [35] modifies the ViT [41] architecture by adding task-specific masked adapters to the Transformer blocks. The masks are also trained using the HAT method.

Firstly, our study novelly recognize the potential of BN in significantly enhancing within-task prediction performance and applies this insight to the CIL paradigm, which has rarely been explored in previous studies. Secondly, our study greatly reduces the number of trainable parameters. The MORE method leverages the HAT approach to train masks that protect important parameters by masking their gradients, preventing updates. However, since gradients for all parameters are calculated before masking, this results in a high computational cost. For instance, MORE uses DeiT-S/16 [42] as the base model, which contains approximately 24 million parameters, all of which require gradient computation. By contrast, our method only sets the BN parameters as trainable with amount of about 15,000 parameters, significantly lower than MORE.

Furthermore, even when only comparing the number of additional mask parameters, MORE requires 70,000 additional parameters for new tasks, which is also significantly higher than our method. Although the number of trainable parameters has been greatly reduced, our method still outperforms MORE in terms of overall performance across multiple datasets, and subsequent experiments will provide further evidence to support this claim.

IV. EXPERIMENTS

A. Experiment setup

We conducted a series of experiments on two medical image datasets, Skin8 [43] and Path16 [16], [44]–[49], as well as a natural image dataset, CIFAR100 [50], to thoroughly validate the effectiveness of our proposed method. These three datasets are all publicly available on the Internet, and their statistics are presented in Table I.

TABLE I: Statistics of three datasets: Skin8, Path16 and CIFAR100. [600, 1024] represents the range of image dimensions in terms of height and width.

Dataset	Number of Classes	Train Set	Test Set	Image Size
Skin8 [43]	8	3,555	705	[600, 1024]
Path16 [16], [44]–[49]	16	12,808	1,607	224 × 224
CIFAR100 [50]	100	50,000	10,000	32 × 32

Skin8 Skin8 [43] is the dataset used in the 2019 skin disease classification challenge hosted by the International Skin Imaging Collaboration. It is a large dataset of skin lesion images sourced from various locations worldwide.

Path16 Path16 [16], [44]–[49] derives from various public pathology datasets, covering a range of disease types and diagnostic scenarios. The dataset statistics are shown in Table II. It includes 7 sub-tasks, each simulating the diagnostic needs for specific diseases in different body parts, such as the stomach and lungs, with high-resolution medical images except Breast and Lymph Node sub-tasks.

TABLE II: Statistics of the Path16 Dataset

Task Name	Number of Classes	Image Size	Train Set	Test Set
Stomach (ST) [16]	4	512×512	630	180
Colon (CO) [44]	2	768×768	630	180
Lung (LU) [44]	2	768×768	630	180
Breast (BR) [45]	2	50×50	630	180
Colorectal Polyps (CP) [46]	2	224×224	630	180
Lymph Node (LN) [47], [48]	2	96×96	630	180
Oral Cavity (OC) [49]	2	2,048×1,538	630	180

CIFAR100 CIFAR100 [50] consists of 60,000 color images at a resolution of 32×32 pixels, distributed across 100 different classes. Each class contains 600 images, with 500 used for training and 100 reserved for testing. The dataset is diverse, containing a wide variety of images, ranging from animals to indoor and outdoor objects in natural scenes.

Hyperparameter Settings For the Path16 and Skin8 datasets, the initial training stage consists of 200 epochs with a batch size of 32. For the optimizer, we utilize Stochastic Gradient

Descent [51] (SGD) with an initial learning rate of 0.01, momentum of 0.9, and weight decay of 0.0005. The learning rate is adjusted according to a multi-step scheduler, dropping to one-tenth of its original value at epochs 70, 130, and 170. The confidence alignment stage lasts for 100 epochs, starting with a learning rate of 0.001 and decreasing to one-tenth at the 55th and 80th epochs. For the CIFAR100 dataset, while maintaining the same optimizer settings and epoch durations in the initial training stage, the batch size is changed to 128 and the weight decay is changed to 0.0002. The confidence alignment stage lasts for 50 epochs, with learning rate reductions at the 15th and 35th epochs.

Data Augmentation Strategies The data preprocessing and augmentation applied to the Path16 dataset includes 50% random horizontal flips, resizing images to 224 × 224, and normalization. The preprocessing on Skin8 dataset mirrors these techniques but we adjust the mean and standard deviation values for normalization to cater to its unique image characteristics. The CIFAR100 dataset introduces a series of augmentations including random cropping, brightness adjustments, and resizing.

Metrics Since the number of samples is class-imbalanced in the Skin8 dataset, we employ Mean Class Recall (MCR) as the evaluation metric to more accurately assess model performance. It is noteworthy that when class distribution is uniform, MCR is equivalent to accuracy, ensuring MCR’s effectiveness across different sample distribution scenarios. The recall rate for a specific class c , α_c , is defined as

$$\alpha_c = \frac{1}{N_c} \sum_{i=1}^{N_c} \mathbf{1}[\hat{y}_i = c], \quad (4)$$

where N_c represents the total number of samples in class c , \hat{y}_i denotes the predicted class for the i -th sample, and c is the actual label of the i -th sample. $\mathbf{1}[\hat{y}_i = c]$ is an indicator function, which is considered correct (value 1) when the predicted class \hat{y}_i matches the actual label c ; otherwise, it is 0. Recall rate α_c measures the performance of a model in correctly identifying instances of class c among all actual instances of class c . Consequently, the model’s MCR after training the t -th task is denoted as MCR_t :

$$\text{MCR}_t = \frac{1}{C_1 + \dots + C_t} \sum_{i=1}^{C_1 + \dots + C_t} \alpha_i, \quad (5)$$

here, C_j represents the number of classes in the j -th task ($j = 1, 2, \dots, t$). MCR_t measures the average recall rate for all classes learned across the t tasks. This ensures that regardless of the number of samples per class, MCR_t fairly evaluates the model’s recognition performance for each class, avoiding potential bias in model evaluation due to imbalanced situations. In the framework of incremental learning, datasets are sequentially divided into T tasks, and MCR can be evaluated at the end of each task phase. Last-MCR is obtained after the final task phase T as $\text{Last-MCR} = \text{MCR}_T$.

Avg-MCR is obtained by calculating MCR at the end of each task phase and then calculating the average of these

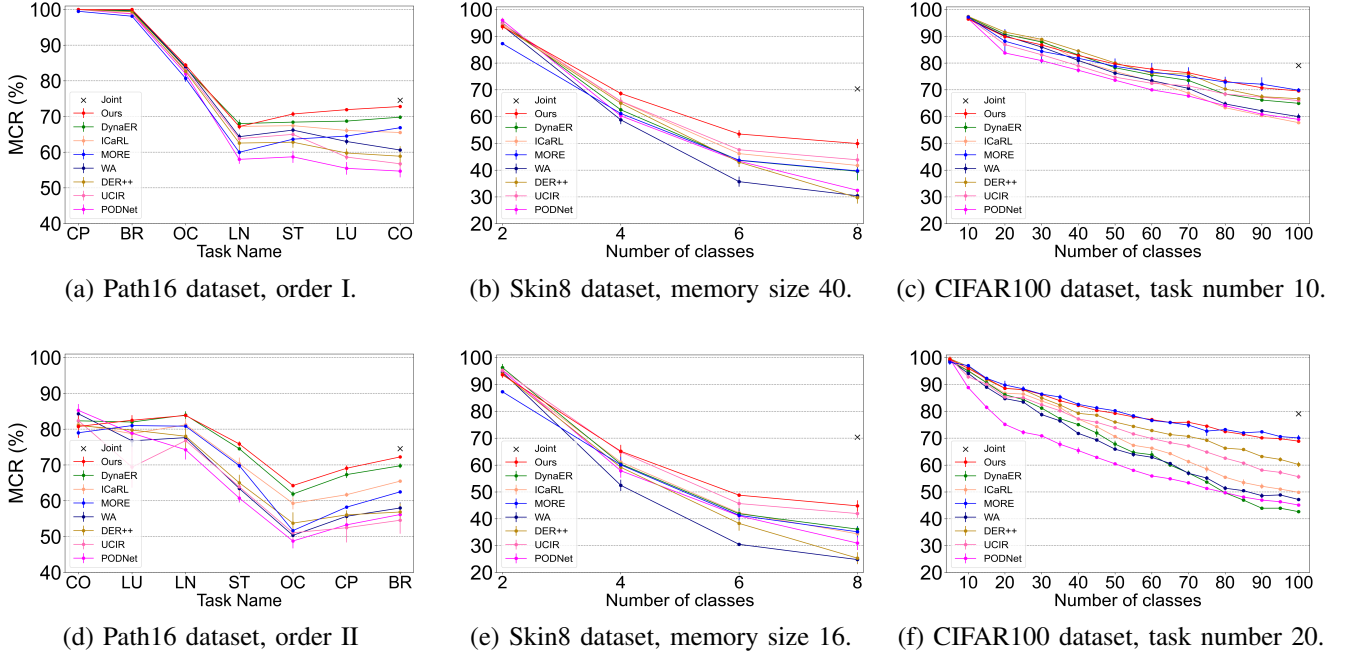


Fig. 3: Performance variation curves of different methods on three datasets under different settings.

TABLE III: Different methods’ performance across three datasets. “Path16-X” refers to the Path16 dataset organized in order X, “Skin8-MX” denotes a memory size of X for the Skin8 dataset, and “CIFAR-XT” indicates the CIFAR dataset divided into X tasks. “Last” and “Avg” respectively represent Last-MCR and Avg-MCR. The “Average” column aggregates the performance across all datasets. The best results are highlighted in bold, the second best are underlined.

Method	Path16-I		Path16-II		Skin8-M40		Skin8-M16		CIFAR100-10T		CIFAR100-20T		Average	
	Last	Avg												
iCaRL	65.52	78.49	65.49	71.16	41.17	62.15	34.40	57.98	57.75	75.74	49.87	71.27	52.37	69.46
UCIR	56.75	75.16	54.56	64.37	<u>43.87</u>	<u>63.02</u>	<u>41.95</u>	<u>61.94</u>	65.99	76.63	55.65	73.95	53.13	69.18
PODNet	54.70	72.52	56.16	65.33	32.47	58.03	30.95	56.27	58.96	73.39	45.12	62.72	46.39	64.71
DynaER	<u>69.45</u>	<u>79.48</u>	<u>69.78</u>	<u>74.54</u>	39.54	60.18	36.15	58.67	64.97	78.59	42.65	67.74	53.76	69.87
WA	60.61	76.85	57.99	66.59	30.44	54.71	24.82	50.59	60.00	76.10	47.18	67.94	46.84	65.46
DER++	58.87	75.15	56.86	67.21	29.73	57.89	25.34	54.18	66.69	<u>79.91</u>	60.21	77.10	49.62	68.57
MORE	66.05	75.84	62.50	69.01	39.72	57.98	35.16	55.95	69.89	79.70	70.09	<u>80.91</u>	<u>57.23</u>	<u>69.90</u>
Ours	73.25	81.00	72.25	75.51	49.93	66.42	44.81	63.08	<u>69.59</u>	80.34	<u>69.81</u>	81.12	63.27	74.58

MCRs after all T task phases are completed. The following equation defines Avg-MCR:

$$\text{Avg-MCR} = \frac{1}{T} \sum_{i=1}^T \text{MCR}_i \quad (6)$$

It is worth noting Last-MCR and Avg-MCR are widely used metrics in incremental learning benchmarks to evaluate the performance of continually knowledge retention and learning.

B. Effectiveness Analysis

Our proposed method was compared with two types of methods within the CIL framework. One type employs task-ID prediction method to apply multi-head TIL methods to the CIL domain, including the MORE [35] method. The other type of method directly targets the CIL domain using single-head approaches, including iCaRL [23], DynaER [9], WA [21], DER++ [25], UCIR [22], and PODNet [20]. The MORE

method employs the DeiT-S [42] as the backbone architecture, whereas all other methods utilize the ResNet18 [12] as backbone. The backbone in all baseline methods have been pretrained on the ImageNet-1K [36] dataset. For memory configuration, the memory size is set to 80 for the Path16 dataset, 40 and 16 respectively for the Skin8 dataset, and 2000 for the CIFAR100 dataset. The results on these datasets are shown in Figure 3 and Table III. The results for each method in the table are averaged over three different random seeds, with variances ranging from 0.10 to 2.08. Additionally, we also report the performance of joint training, which involves training the model on data of all tasks simultaneously, representing the theoretical upper bound of model performance, marked with “x” in the figures.

On the Path16 dataset, to comprehensively evaluate the model’s performance under various task orders, we randomly sets two different task orders. Each order represents a pathway of incremental learning, with each task corresponding to a

specific subset within Path16. Specifically, task order I is CP \rightarrow BR \rightarrow OC \rightarrow LN \rightarrow ST \rightarrow LU \rightarrow CO, and task order II is CO \rightarrow LU \rightarrow LN \rightarrow ST \rightarrow OC \rightarrow CP \rightarrow BR. The results are shown in the Figure 3(a) and Figure 3(d) and in the Path16-I and Path16-II columns of the Table III. The figures demonstrate that under both task orders of the Path16 medical dataset, our proposed method consistently outperforms the baseline methods. Specifically, under different task orders, the final performance (Last-MCR) of our proposed method stabilized at around 73%, approaching the performance upper bound of Joint at 74.55%. In task order I, which progresses from simpler tasks (CP and BR), the performance of all methods was nearly 100% initially. As the OC and LN tasks were introduced, the performance of baseline methods generally declined, while our proposed method maintained the lead. In the later stages of incremental learning, from the LN task to the CO task, our method showed performance improvements on these specific tasks, which led to an overall increase in the average performance across all tasks. The results shows that on the Path16 dataset, DynaER performed second best, with Last-MCR and Avg-MCR reaching 69.45% and 79.48%, respectively, yet our method still showed performance improvements of 3.80% and 1.52% over DynaER, respectively. Similar findings were observed under task order II.

On the Skin8 dataset, with memory sizes of 40 and 16 and the number of tasks (T) set to 4, the results are displayed in Figure 3(b) and Figure 3(e), as well as in the columns Skin8-M40 and Skin8-M16 of Table III. These results show that under both memory size settings, our method consistently maintained the best performance. With a memory size of 40, Last-MCR reached 49.93% and Avg-MCR reached 66.42%, showing improvements of 6.06% and 3.40% over the second best method, UCIR, which had Last-MCR at 43.87% and Avg-MCR at 63.02%, respectively. The performance under both memory settings confirms that our method is not sensitive to the size of the memory, maintaining best performance.

The effectiveness of our proposed method is demonstrated not only on medical image datasets but also on natural image datasets. When the number of tasks (T) was set to 10 and 20, the results are shown in Figure 3(c) and Figure 3(f) and in the CIFAR100-10T and CIFAR100-20T columns of Table III. Our method achieved the best performance in Avg-MCR at 80.34% and 81.12%, and second best in Last-MCR at 69.89% and 70.09%, respectively, with only a slight difference of 0.30% and 0.28% from the top-performing MORE method.

Further comparing our proposed method with the similar method MORE, it can be observed that our method outperforms MORE on most of the incremental learning settings across the majority of datasets, while being comparable performance on a few settings. On medical image datasets, the inferior performance of MORE is due to a certain degree of overfitting when the sample size is small. For example, on the initial task of the Skin8 dataset, the accuracy of MORE on the training set reaches 97.79%, while its test accuracy is only 86.71%. Similar results are observed in other tasks as well for our method and MORE. Additionally, MORE uses a random selection method to

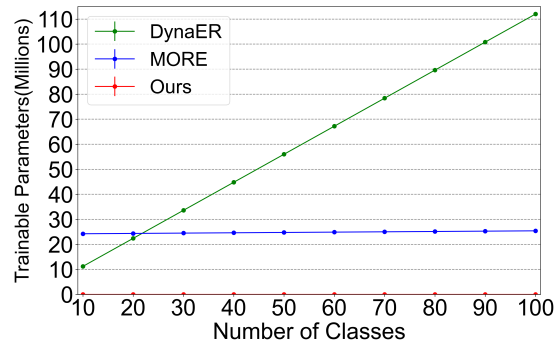


Fig. 4: Comparison of parameter increase between the proposed method and the best-performing baseline methods, DynaER and MORE, on the CIFAR100 dataset with 10 tasks.

select old samples for replay, which selects less representative samples comparing to the herding selection method [23] that we use when the sample set is small. In summary, in terms of average performance across the three datasets, our proposed method not only shows significant improvement compared to the MORE method but also demonstrates substantial gains over all baseline methods.

Parameter Growth Analysis To more intuitively compare the growth in the number of parameters of our method with those of the baseline methods with the progress of incremental learning, we conducted comparisons between our proposed method and the best-performing baseline methods, DynaER and MORE. As observed in Figure 4, with each incoming task, DynaER experiences a substantial growth of 11.2 million parameters, significantly increasing the resource consumption of the training stage. Although the MORE method does not exhibit significant parameter growth, it still calculates gradients for all parameters in the model. To protect important parameters, it applies masks to zero out the gradients of these parameters. This results in a significant computational cost due to the need to compute gradients for the entire model. Furthermore, these masks are task-specific, with each mask requiring approximately 70,000 parameters. In contrast, our method exhibits a minimal increase of only 15,000 parameters with the arrival of each task, which is negligible compared to the total number of backbone parameters. Our method not only significantly reduce the number of used parameters, but also consistently outperforms all other methods in terms of performance across three datasets.

C. Generalizabilization Assessment

To investigate the generalization ability of the method proposed in this study, we utilized ResNet34 and ResNet50 architectures to further compare with selected baseline methods DynaER and iCaRL. It is noteworthy that although the MORE method performed well among the baselines, it is dependent on a Transformer network and is not adaptable to other ResNet architectures. Therefore, MORE was excluded from this comparison, and only the best-performing methods

TABLE IV: Comparison of the proposed method with baseline methods on three datasets with three backbone networks. Specifically, experiments on the Path16 dataset were conducted under task order I, on CIFAR100 under a division into 10 tasks, and on Skin8 with a memory setting of 40. “Last” and “Avg” represent Last-MCR and Avg-MCR, respectively.

Dataset	Method	ResNet18		ResNet34		ResNet50	
		Last	Avg	Last	Avg	Last	Avg
Path16	iCaRL	65.52 \pm 0.34	78.49 \pm 0.56	65.16 \pm 1.41	78.47 \pm 0.03	64.75 \pm 1.36	78.81 \pm 0.57
	DynaER	69.45 \pm 0.34	79.48 \pm 0.54	69.95 \pm 1.41	79.57 \pm 0.49	69.09 \pm 1.15	79.31 \pm 0.19
	Ours	73.41\pm0.34	81.23\pm0.41	73.78\pm1.01	81.58\pm0.57	75.11\pm0.97	82.30\pm0.59
CIFAR100	iCaRL	57.75 \pm 0.35	75.74 \pm 0.18	60.08 \pm 0.24	76.89 \pm 0.17	60.03 \pm 0.22	76.80 \pm 0.17
	DynaER	64.97 \pm 0.68	78.59 \pm 0.22	44.49 \pm 1.35	68.92 \pm 0.47	47.58 \pm 1.13	71.13 \pm 0.60
	Ours	69.59\pm0.33	80.34\pm0.17	72.10\pm0.52	79.66\pm1.24	73.52\pm0.14	81.17\pm1.10
Skin8	iCaRL	41.17 \pm 1.42	62.15 \pm 0.40	41.00 \pm 1.61	56.40 \pm 0.52	40.95 \pm 0.14	57.41 \pm 0.37
	DynaER	39.54 \pm 3.35	60.18 \pm 1.46	41.19 \pm 1.18	60.89 \pm 0.50	36.56 \pm 2.83	58.33 \pm 1.17
	Ours	49.93\pm1.73	66.42\pm1.08	51.07\pm2.09	68.18\pm1.33	52.87\pm0.92	68.48\pm1.23

among the remaining baselines, DynaER and iCaRL, were selected for further analysis. The results are presented in Table IV.

It can be observed that our method consistently maintained superior performance across different architectures. Moreover, as the network depth increased, our method demonstrated performance improvements on all three datasets. Specifically, when upgrading from ResNet18 to ResNet50, the Last-MCR for Path16, CIFAR100, and Skin8 datasets increased by 1.70%, 3.93%, and 3.84% respectively, while the Avg-MCR increased by 1.07%, 0.83%, and 2.06% respectively. In contrast, iCaRL’s performance remained basically unchanged across different architectures. On the other hand, DynaER’s performance showed inconsistent trends across different datasets, with fluctuating performances on Path16 and Skin8, and a significant decrease on CIFAR100, indicating a sensitivity to the network architecture employed.

D. Ablation Study

The proposed method comprises three parts, and the results of ablation studies on these parts are shown in Table V. The results shown in the table are the average result from results with three different random seeds, with variances ranging from 0.01 to 0.45. “T.S.BN” refers to the use of task-specific batch normalization. Its removal implies the shared use of pretrained model’s batch normalization layers across tasks, with only the task-specific classification heads being trainable upon the arrival of new tasks. “Unknown” denotes the addition of an “unknown” class in the classification head. Removing it means that the prediction of the task-ID can only rely on the highest output score among classes, without utilizing the output score of the unknown class. “Alignment” refers to the OOD Detection Capability Alignment Stage, during which it is also essential to utilize the design of the “Unknown”.

From the first row in Table V, it is evident that using only task-specific BN leads to a significant performance drop. This is because the model still gives high outputs for samples not belonging to the task, thereby reducing the performance of task-ID prediction. This highlights the beneficial impact of the “Unknown” Class and “Alignment” on enhancing task-ID prediction. The second row reveals that even with the use

of task-specific BN and the addition of an “unknown” class in the classification heads, performance remains poor due to the absence of the alignment stage. This situation results in the classification head of the first task never encountering OOD samples, thus always producing a zero output for the “unknown” class and biasing the task-ID prediction towards the first task. This further emphasizes the critical role of the “Alignment” in task-ID prediction. According to the third row, employing both “Unknown” and the “Alignment” to ensure task-ID prediction performance still shows a decrease in performance, which underscores the importance of “Task-specific BN” in enhancing within-task prediction performance. In summary, task-specific BN enhances performance in task-specific sub-models for within-task prediction, while the addition of an unknown class and the alignment stage for OOD capability significantly boost task-ID prediction performance in task-specific sub-models, eventually to a better final incremental learning performance.

Components			Path16		CIFAR100	
T.S.BN	Unknown	Alignment	Last	Avg	Last	Avg
✓			18.61	44.25	17.20	42.66
✓	✓		12.45	35.21	9.66	28.29
	✓	✓	66.43	77.39	66.43	77.39
✓	✓	✓	73.25	81.09	69.59	80.34

TABLE V: The ablation study results of the proposed method. “T.S.BN” stands for task-specific Batch Normalization. “Unknown” refers to the addition of an unknown class in the classification head, and “Alignment” denotes the OOD confidence alignment stage. “Last” and “Avg” respectively represent Last-MCR and Avg-MCR.

V. CONCLUSION AND FUTURE WORK

To address the catastrophic forgetting problem and achieve a better balance between stability, plasticity, and parameter growth, we proposed a class incremental learning method based on task-specific batch normalization and classification heads combined with OOD detection. This method has reached the state-of-the-art performance on the medical image datasets Skin8, Path16, and the natural image dataset CIFAR100. The generalization experiments further confirmed the adaptability

of our method across models with different scales, and ablation studies validated the effectiveness of each component. In conclusion, our method efficiently and effectively mitigates model forgetting and keep the model's plasticity with very few model parameter growth. For future work, we plan to integrate more advanced OOD detection methods to achieve more accurate task-ID prediction and further enhance model performance.

REFERENCES

- [1] R. M. French, "Catastrophic forgetting in connectionist networks," *Trends in Cognitive Sciences*, vol. 3, no. 4, pp. 128–135, 1999. **1**
- [2] X. Xie, J. Xu, P. Hu, W. Zhang, Y. Huang, W. Zheng, and R. Wang, "Task-incremental medical image classification with task-specific batch normalization," in *Chinese Conference on Pattern Recognition and Computer Vision*, 2023, pp. 309–320. **1, 2**
- [3] A. Chaudhry, P. K. Dokania, T. Ajanthan, and P. H. Torr, "Riemannian walk for incremental learning: Understanding forgetting and intransigence," in *Proceedings of the European Conference on Computer Vision*, 2018, pp. 532–547. **1, 2**
- [4] J. Kirkpatrick, R. Pascanu, N. Rabinowitz, J. Veness, G. Desjardins, A. A. Rusu, K. Milan, J. Quan, T. Ramalho, and A. Grabska-Barwinska, "Overcoming catastrophic forgetting in neural networks," *Proceedings of the National Academy of Sciences of the United States of America*, vol. 114, pp. 3521–3526, 2017. **1, 2**
- [5] R. Aljundi, F. Babiloni, M. Elhoseiny, M. Rohrbach, and T. Tuytelaars, "Memory aware synapses: Learning what (not) to forget," in *Proceedings of the European Conference on Computer Vision*, 2018, pp. 139–154. **1, 2**
- [6] A. A. Rusu, N. C. Rabinowitz, G. Desjardins, H. Soyer, J. Kirkpatrick, K. Kavukcuoglu, R. Pascanu, and R. Hadsell, "Progressive neural networks," in *International Conference on Learning Representations*, 2016. **1, 3**
- [7] C. Fernando, D. Banarse, C. Blundell, Y. Zwols, D. Ha, A. A. Rusu, A. Pritzel, and D. Wierstra, "PathNet: Evolution channels gradient descent in super neural networks," *arXiv preprint arXiv:1701.08734*, 2017. **1, 3**
- [8] A. Douillard, A. Ramé, G. Couairon, and M. Cord, "DyTox: Transformers for continual learning with dynamic token expansion," in *Proceedings of the IEEE Conference on Computer Vision and Pattern Recognition*, 2022, pp. 9285–9295. **1, 3**
- [9] S. Yan, J. Xie, and X. He, "DER: Dynamically expandable representation for class incremental learning," in *Proceedings of the IEEE Conference on Computer Vision and Pattern Recognition*, 2021, pp. 3014–3023. **1, 2, 3, 7**
- [10] W. Zhang, Y. Huang, T. Zhang, Q. Zou, W.-S. Zheng, and R. Wang, "Adapter learning in pretrained feature extractor for continual learning of diseases," in *International Conference on Medical Image Computing and Computer-Assisted Intervention*, 2023, pp. 68–78. **1**
- [11] S. Ioffe and C. Szegedy, "Batch normalization: Accelerating deep network training by reducing internal covariate shift," in *Proceedings of the International Conference on Machine Learning*, 2015, pp. 448–456. **2**
- [12] K. He, X. Zhang, S. Ren, and J. Sun, "Deep residual learning for image recognition," in *Proceedings of the IEEE Conference on Computer Vision and Pattern Recognition*, 2016, pp. 770–778. **2, 7**
- [13] T. Karras, S. Laine, and T. Aila, "A style-based generator architecture for generative adversarial networks," in *Proceedings of the IEEE Conference on Computer Vision and Pattern Recognition*, 2019, pp. 4401–4410. **2, 3**
- [14] Y.-C. Hsu, Y.-C. Liu, A. Ramasamy, and Z. Kira, "Re-evaluating continual learning scenarios: A categorization and case for strong baselines," *arXiv preprint arXiv:1810.12488*, 2018. **2**
- [15] G. M. Van de Ven and A. S. Tolias, "Three scenarios for continual learning," *arXiv preprint arXiv:1904.07734*, 2019. **2**
- [16] Y. Yang, Z. Cui, J. Xu, C. Zhong, W.-S. Zheng, and R. Wang, "Continual learning with bayesian model based on a fixed pre-trained feature extractor," *Visual Intelligence*, vol. 1, p. 5, 2023. **2, 6**
- [17] L. Wang, X. Zhang, H. Su, and J. Zhu, "A comprehensive survey of continual learning: Theory, method and application," *IEEE Transactions on Pattern Analysis and Machine Intelligence*, 2024. **2**
- [18] Y. Qiu, Y. Shen, Z. Sun, Y. Zheng, X. Chang, W. Zheng, and R. Wang, "Sats: Self-attention transfer for continual semantic segmentation," *Pattern Recognition*, vol. 138, p. 109383, 2023. **2**
- [19] Z. Li and D. Hoiem, "Learning without forgetting," *IEEE Transactions on Pattern Analysis and Machine Intelligence*, vol. 40, no. 12, pp. 2935–2947, 2017. **2**
- [20] A. Douillard, M. Cord, C. Ollion, T. Robert, and E. Valle, "PODNet: Pooled outputs distillation for small-tasks incremental learning," in *Proceedings of the European Conference on Computer Vision*, 2020, pp. 86–102. **2, 7**
- [21] B. Zhao, X. Xiao, G. Gan, B. Zhang, and S.-T. Xia, "Maintaining discrimination and fairness in class incremental learning," in *Proceedings of the IEEE Conference on Computer Vision and Pattern Recognition*, 2020, pp. 13 208–13 217. **2, 7**
- [22] S. Hou, X. Pan, C. C. Loy, Z. Wang, and D. Lin, "Learning a unified classifier incrementally via rebalancing," in *Proceedings of the IEEE Conference on Computer Vision and Pattern Recognition*, 2019, pp. 831–839. **2, 7**
- [23] S.-A. Rebuffi, A. Kolesnikov, G. Sperl, and C. H. Lampert, "iCaRL: Incremental classifier and representation learning," in *Proceedings of the IEEE Conference on Computer Vision and Pattern Recognition*, 2017, pp. 2001–2010. **2, 5, 7, 8**
- [24] M. PourKeshavarzi, G. Zhao, and M. Sabokrou, "Looking back on learned experiences for class/task incremental learning," in *International Conference on Learning Representations*, 2022. **2**
- [25] P. Buzzega, M. Boschini, A. Porrello, D. Abati, and S. Calderara, "Dark experience for general continual learning: a strong, simple baseline," *Advances in neural information processing systems*, vol. 33, pp. 15 920–15 930, 2020. **2, 7**
- [26] R. Aljundi, M. Lin, B. Goujaud, and Y. Bengio, "Gradient based sample selection for online continual learning," *Advances in Neural Information Processing Systems*, vol. 32, 2019. **2**
- [27] D. Abati, J. Tomczak, T. Blankevoort, S. Calderara, R. Cucchiara, and B. E. Bejnordi, "Conditional channel gated networks for task-aware continual learning," in *Proceedings of the IEEE Conference on Computer Vision and Pattern Recognition*, 2020, pp. 3931–3940. **3**
- [28] J. von Oswald, C. Henning, B. F. Grewe, and J. Sacramento, "Continual learning with hypernetworks," in *International Conference on Learning Representations*, 2020. **3**
- [29] C. Henning, M. Cervera, F. D'Angelo, J. Von Oswald, R. Traber, B. Ehret, S. Kobayashi, B. F. Grewe, and J. Sacramento, "Posterior meta-replay for continual learning," *Advances in Neural Information Processing Systems*, vol. 34, pp. 14 135–14 149, 2021. **3**
- [30] J. Rajasegaran, S. Khan, M. Hayat, F. S. Khan, and M. Shah, "iTAML: An incremental task-agnostic meta-learning approach," in *Proceedings of the IEEE Conference on Computer Vision and Pattern Recognition*, 2020, pp. 13 588–13 597. **3**
- [31] G. Kim, C. Xiao, T. Konishi, Z. Ke, and B. Liu, "A theoretical study on solving continual learning," *Advances in Neural Information Processing Systems*, vol. 35, pp. 5065–5079, 2022. **3, 5**
- [32] J. Guérin, K. Delmas, R. Ferreira, and J. Guiochet, "Out-of-distribution detection is not all you need," in *Proceedings of the AAAI Conference on Artificial Intelligence*, 2023, pp. 14 829–14 837. **3**
- [33] W. Liu, X. Wang, J. Owens, and Y. Li, "Energy-based out-of-distribution detection," *Advances in Neural Information Processing Systems*, vol. 33, pp. 21 464–21 475, 2020. **3**
- [34] Z. Sun, Y. Qiu, Z. Tan, W. Zheng, and R. Wang, "Classifier-head informed feature masking and prototype-based logit smoothing for out-of-distribution detection," *IEEE Transactions on Circuits and Systems for Video Technology*, pp. 1–1, 2024. **3**
- [35] G. Kim, B. Liu, and Z. Ke, "A multi-head model for continual learning via out-of-distribution replay," in *Conference on Lifelong Learning Agents*, 2022, pp. 548–563. **3, 5, 7**
- [36] J. Deng, W. Dong, R. Socher, L.-J. Li, K. Li, and L. Fei-Fei, "Imagenet: A large-scale hierarchical image database," in *Proceedings of the IEEE Conference on Computer Vision and Pattern Recognition*, 2009, pp. 248–255. **3, 7**
- [37] T. Karras, M. Aittala, S. Laine, E. Härkönen, J. Hellsten, J. Lehtinen, and T. Aila, "Alias-free generative adversarial networks," *Advances in Neural Information Processing Systems*, 2021. **3**
- [38] A. Bendale and T. E. Boulton, "Towards open set deep networks," in *Proceedings of the IEEE Conference on Computer Vision and Pattern Recognition*, 2016, pp. 1563–1572. **5**
- [39] J. Serra, D. Suris, M. Miron, and A. Karatzoglou, "Overcoming catastrophic forgetting with hard attention to the task," in *Proceedings of the International Conference on Machine Learning*, 2018, pp. 4548–4557. **5**
- [40] J. Tack, S. Mo, J. Jeong, and J. Shin, "Csi: Novelty detection via contrastive learning on distributionally shifted instances," *Advances in*

- Neural Information Processing Systems*, vol. 33, pp. 11 839–11 852, 2020. 5
- [41] A. Dosovitskiy, L. Beyer, A. Kolesnikov, D. Weissenborn, X. Zhai, T. Unterthiner, M. Dehghani, M. Minderer, G. Heigold, S. Gelly, J. Uszkoreit, and N. Houlsby, “An image is worth 16x16 words: Transformers for image recognition at scale,” in *International Conference on Learning Representations*, 2021. 5
- [42] H. Touvron, M. Cord, M. Douze, F. Massa, A. Sablayrolles, and H. Jégou, “Training data-efficient image transformers & distillation through attention,” in *Proceedings of the International Conference on Machine Learning*, 2021, pp. 10 347–10 357. 5, 7
- [43] P. Tschandl, C. Rosendahl, and H. Kittler, “The ham10000 dataset, a large collection of multi-source dermatoscopic images of common pigmented skin lesions,” *Scientific data*, vol. 5, p. 180161, 2018. 6
- [44] A. A. Borkowski, M. M. Bui, L. B. Thomas, C. P. Wilson, L. A. DeLand, and S. M. Mastorides, “Lung and colon cancer histopathological image dataset (lc25000),” *arXiv preprint arXiv:1912.12142*, 2019. 6
- [45] A. Janowczyk and A. Madabhushi, “Deep learning for digital pathology image analysis: A comprehensive tutorial with selected use cases,” *Journal of Pathology Informatics*, vol. 7, no. 1, p. 29, 2016. 6
- [46] J. Wei, A. Suriawinata, B. Ren, X. Liu, M. Lisovsky, L. Vaickus, C. Brown, M. Baker, N. Tomita, and L. Torresani, “A petri dish for histopathology image analysis,” in *Artificial Intelligence in Medicine*, 2021, pp. 11–24. 6
- [47] B. S. Veeling, J. Linmans, J. Winkens, T. Cohen, and M. Welling, “Rotation equivariant cnns for digital pathology,” in *International Conference on Medical Image Computing and Computer Assisted Intervention*, 2018, pp. 210–218. 6
- [48] B. E. Bejnordi, M. Veta, P. J. Van Diest, B. Van Ginneken, N. Karssemeijer, G. Litjens, J. A. Van Der Laak, M. Hermsen, Q. F. Manson, and M. Balkenhol, “Diagnostic assessment of deep learning algorithms for detection of lymph node metastases in women with breast cancer,” *Journal of the American Medical Association*, vol. 318, no. 22, pp. 2199–2210, 2017. 6
- [49] A. F. Kebede, “Oral cancer dataset, version 1,” Kaggle, 2021. [Online]. Available: <https://www.kaggle.com/datasets/ashenafasilkebede/dataset> 6
- [50] A. Krizhevsky and G. Hinton, “Learning multiple layers of features from tiny images,” *Technical report, University of Toronto*, vol. 4, no. 7, 2009. 6
- [51] S.-i. Amari, “Backpropagation and stochastic gradient descent method,” *Neurocomputing*, vol. 5, pp. 185–196, 1993. 6